# A 26 million year gap in the central Arctic record at the greenhouse-icehouse transition: Looking for clues

Francesca Sangiorgi,[1,2] Hans-Jürgen Brumsack,[3] Debra A. Willard,[4] Stefan Schouten,[2] Catherine E. Stickley,[5] Matthew O'Regan,[6] Gert-Jan Reichart,[7] Jaap S. Sinninghe Damsté,[2,7] and Henk Brinkhuis[1]

Received 29 April 2007; revised 7 October 2007; accepted 17 October 2007; published 29 February 2008.

[1] The Cenozoic record of the Lomonosov Ridge (central Arctic Ocean) recovered during Integrated Ocean Drilling Program (IODP) Expedition 302 revealed an unexpected 26 Ma hiatus, separating middle Eocene (~44.4 Ma) from lower Miocene sediments (~18.2 Ma). To elucidate the nature of this unconformity, we performed a multiproxy palynological (dinoflagellate cysts, pollen, and spores), micropaleontological (siliceous microfossils), inorganic, and organic (Tetra Ether Index of lipids with 86 carbon atoms ($TEX_{86}$) and Branched and Isoprenoid Tetraether (BIT)) geochemical analysis of the sediments from ~5 m below to ~7 m above the hiatus. Four main paleoenvironmental phases (A–D) are recognized in the sediments encompassing the unconformity, two below (A–B) and two above (C–D): (A) Below the hiatus, proxies show relatively warm temperatures, with Sea Surface Temperatures ($TEX_{86}$-derived SSTs) of about 8°C and high fresh to brackish water influence. (B) Approaching the hiatus, proxies indicate a cooling trend ($TEX_{86}$-derived SSTs of ~5°C), increased freshwater influence, and progressive shoaling of the Lomonosov Ridge drilling site, located close to or at sea level. (C) The interval directly above the unconformity contains sparse reworked Cretaceous to Oligocene dinoflagellate cysts. Sediments were deposited in a relatively shallow, restricted marine environment. Proxies show the simultaneous influence of both fresh and marine waters, with alternating oxic and anoxic conditions. Pollen indicates a relatively cold climate. Intriguingly, $TEX_{86}$-derived SSTs are unexpectedly high, ~15–19°C. Such warm surface waters may be partially explained by the ingression of warmer North Atlantic waters after the opening of the Fram Strait during the early Miocene. (D) Sediments of the uppermost interval indicate a phase of extreme oxic conditions, and a well-ventilated environment, which occurred after the complete opening of the Fram Strait. Importantly, and in contrast with classical postrifting thermal subsidence models for passive margins, our data suggest that sediment erosion and/or nondeposition that generated the hiatus was likely due to a progressive shoaling of the Lomonosov Ridge. A shallow water setting both before and after the hiatus suggests that the Lomonosov Ridge remained at or near sea level for the duration of the gap in the sedimentary record. Interacting sea level changes and/or tectonic activity (possibly uplift) must be invoked as possible causes for such a long hiatus.

**Citation:** Sangiorgi, F., H.-J. Brumsack, D. A. Willard, S. Schouten, C. E. Stickley, M. O'Regan, G.-J. Reichart, J. S. Sinninghe Damsté, and H. Brinkhuis (2008), A 26 million year gap in the central Arctic record at the greenhouse-icehouse transition: Looking for clues, *Paleoceanography*, *23*, PA1S04, doi:10.1029/2007PA001477.

## 1. Introduction

[2] The first Cenozoic record from the central Arctic Ocean was acquired in 2004 during Integrated Ocean Drilling Program (IODP) Expedition 302 (the Arctic Coring Expedition (ACEX)) from core holes drilled 250 km from the North Pole [*Expedition 302 Scientists*, 2006]. The cores were recovered in water depths of ~1300 m by drilling of the crest of the Lomonosov Ridge. About 428 m of partially recovered sediments have provided the first biostratigraphic and paleoenvironmental insights into the Cenozoic history of the Arctic Ocean. The recognition of a major mid-Cenozoic hiatus was initially noted during the expedition [*Expedition 302 Scientists*, 2006]. Later, *Moran et al.* [2006] reported the occurrence of "a presumably condensed and possibly partially missing section from ~44 to 16 Ma". Detailed biostratigraphic studies, based primarily on organic

[1]Laboratory of Palaeobotany and Palynology, Utrecht University, Utrecht, Netherlands.
[2]Department of Marine Biogeochemistry and Toxicology, Royal Netherlands Institute for Sea Research (NIOZ), Texel, Netherlands.
[3]Institute for Chemistry and Biology of the Marine Environment (ICBM), Oldenburg University, Oldenburg, Germany.
[4]U.S. Geological Survey, Reston, Virginia, USA.
[5]Norwegian Polar Institute, Polar Environmental Centre, Tromsø, Norway.
[6]Graduate School of Oceanography University of Rhode Island, Narragansett, Rhode Island, USA.
[7]Department of Earth Sciences, Utrecht University, Utrecht, Netherlands.


0883-8305/08/2007PA001477

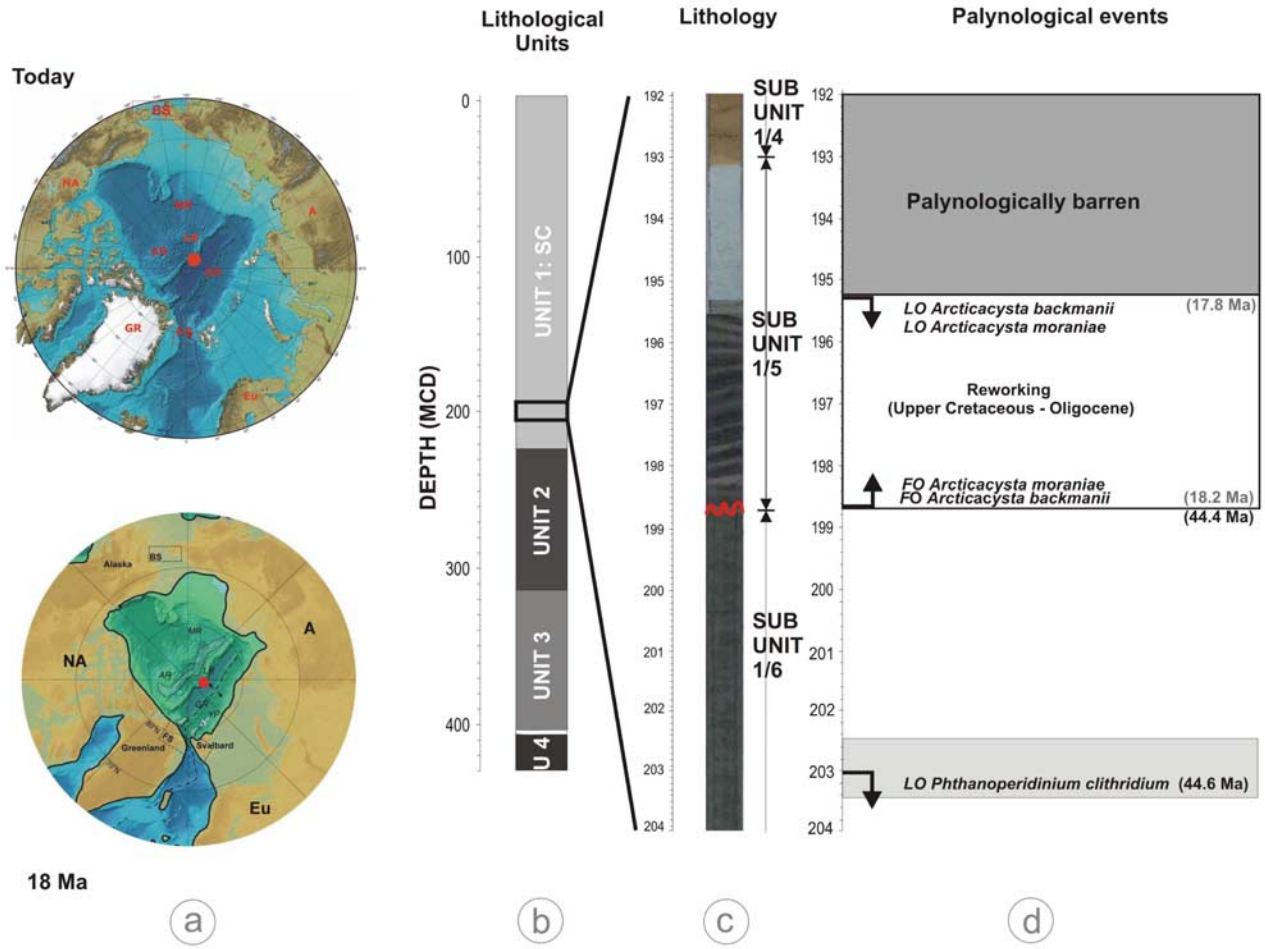


**Figure 1.** (a) (top) Location of the Arctic Coring Expedition (ACEX) drilling sites on the Lomonosov Ridge (LR) indicated on the International Bathymetric Chart of the Arctic Ocean (modified from http://www.ngdc.noaa.gov/mgg/bathymetry/arctic/arctic.html). (bottom) Location of the ACEX drilling sites on the Lomonosov Ridge (LR) indicated an 18 Ma paleogeographic/paleobathymetric reconstruction [modified from *Jakobsson et al.*, 2007]. Gr: Greenland; NA: North America; A: Asia; Eu: Europe; FS: Fram Strait; BS: Bering Strait; GR: Gakkel Ridge; AR: Alpha Ridge; MR: Mendeleev Ridge; YP: Yermak Plateau. (b, c) Lithostratigraphic column, with the indication of the four lithologic units recognized in the section (Figure 1b) [*Expedition 302 Scientists*, 2006] and image of the core section, which contains the hiatus (red wiggly line) and the "zebra" interval above it (Figure 1c); (d) Dinocyst events, which permitted the identification of the hiatus and its duration: Last Occurrence (LO) of *Phthanoperidinium clithridium* (44.6 Ma) [*Eldrett et al.*, 2004], First Occurrence of the dinocysts belonging to the genus *Arcticacysta* marking the palynological break at 198.70 mcd (18.2 Ma) [*Sangiorgi et al.*, 2008], and its Last Occurrence in the ACEX record (~17.8 Ma), based on the ACEX age model [*Backman et al.*, 2008]. Light gray rectangle indicates an interval with well-preserved siliceous microfossils (see text and *Stickley et al.* [2008]).

walled dinoflagellate cysts (dinocysts), have subsequently provided evidence that the hiatus lasted ~26 Ma, from the middle Eocene (~44.4 Ma) to the late early Miocene (~18.2 Ma) [*Backman et al.*, 2008; *Sangiorgi et al.*, 2008].

[3] The hiatus separates two very different sedimentary regimes of the Paleogene and the Neogene. Paleogene sediments are dark, partly laminated, siliciclastic claystones rich in organic carbon (TOC up to 5%), pyrite, and microfossils. The Neogene sediments are generally silty muds, poor in organic carbon and microfossils but containing abundant dropstones and sand lenses [*Expedition 302 Scientists*, 2006; *Moran et al.*, 2006].

[4] The unconformity, masked in the seismic profile, occurs at an abrupt change in sediment color, between subunit 1/6 and subunit 1/5 (core M0002A-46X 1W, at 198.70 meters composite depth, mcd) of the ACEX record [*Sangiorgi et al.*, 2008] (Figure 1). Subunit 1/6 is characterized by dark brown silty clays and contains a middle Eocene dinocyst marker species (*Phthanoperidinium clithridium*). This contrasts with subunit 1/5, a 5.7 m interval, in which the lower part is characterized by ~2.5 m of black to

dark gray, alternating clayey bands (informally called the "zebra" interval) and a distinctive dinocyst assemblage dominated by a new dinocyst genus (*Arcticacysta*) of late early Miocene age. Lower subunit 1/5 contains also sparse reworked dinocysts of Cretaceous to Oligocene age [*Sangiorgi et al.*, 2008]. The hiatus marks an abrupt decrease in sedimentation rates, from 24.3 m/Ma in the middle Eocene to 8.0 m/Ma in the early Miocene [*Backman et al.*, 2008].

[5] In an attempt to examine the possible causes for the 26 Ma hiatus we have undertaken a high-resolution multiproxy study (dinocysts, pollen and spores, siliceous microfossils, inorganic and organic geochemistry) paleoenvironmental reconstruction of adjacent sediments, from ~5 m below to ~7 m above the unconformity.

## 2. Material and Methods

[6] Sediment cores from the Lomonosov Ridge, central Artic Ocean (Figure 1), were recovered from four closely spaced drill holes with minimal stratigraphic overlap. A single composite stratigraphic section was constructed, and four lithological units were defined in the ACEX sediment core sequence, on the basis of visual, textural, and compositional properties and geochemical analyses. Unit 1 includes the upper 223.6 m of siliciclastic sediments (silty clays to clayey silts) ranging from late middle Eocene to Holocene age. Unit 1 has been further subdivided into six subunits, defined mainly on sediment color and geochemical parameters such as biogenic carbonate and silica, total organic carbon (TOC), and pyrite content (for details, see *Expedition 302 Scientists* [2006] and *Moran et al.* [2006]). The transition between subunit 1/6 and 1/5 (198.70 mcd, Figure 1) corresponds to the hiatus [*Backman et al.*, 2008; *Sangiorgi et al.*, 2008]. The sedimentary record shows no obvious unconformity, and the division in the two subunits was based solely on changes in color and in pyrite content [*Expedition 302 Scientists*, 2006; *Moran et al.*, 2006].

[7] Our analysis focuses on the upper part of subunit 1/6, subunit 1/5, and the lower part of subunit 1/4 (cores M0002A-47X 3W to M0002A-44X 1W) extending from 203.70 to 191.99 mcd (Figure 1). The sediments of subunit 1/6 are homogeneous, dark, organic-rich, siliceous clays with high pyrite content and TOC of 2–4%. Lower subunit 1/5 is characterized by alternating black to dark gray, centimeter-wide "zebra" clayey bands, with TOC up to 14%. Upper subunit 1/5 consists of olive gray to light gray clays with TOC lower than 1%, and lower subunit 1/4 consists of red clays, with TOC < 0.2 % [*Expedition 302 Scientists*, 2006; *Moran et al.*, 2006; *Stein et al.*, 2006]. The upper subunit 1/5 (above 195.30 mcd) and lower subunit 1/4 are palynologically barren [*Sangiorgi et al.*, 2008] (Figure 1).

### 2.1. Age Assessment and the Duration of the Hiatus

[8] The upper part of subunit 1/6 contains the Last Occurrence (LO) of the dinocyst *Phthanoperidinium clithridium*, at 200.49 mcd. This event has been dated at 44.6 Ma in the Norwegian-Greenland Sea [*Eldrett et al.*, 2004] using the timescales of *Cande and Kent* [1995]. Because dinocysts are sparse in the ~3 m below the hiatus, we prefer to use the Last Abundant Occurrence (LAO) of *P. clithridium* at 203 mcd as its LO (Figure 1). Considering a sedimentation rate in this interval of about 24.3 m/Ma [see *Backman et al.*, 2008] and using a linear extrapolation, the age of the youngest sediment beneath the hiatus is ~44.4 Ma.

[9] Just above the hiatus, in subunit 1/5, two dinocyst species, belonging to the new genus *Arcticacysta* (*A. backmanii* and *A. moraniae*) [*Sangiorgi et al.*, 2008] have their First Occurrence (FO) (Figure 1). In this subunit there are also sparse reworked dinocysts, ranging in age from the Cretaceous to the Oligocene [see also *Expedition 302 Scientists*, 2006]. On the basis of the sporadic reworking, and because dinocyst taxa, closely resembling the *Arcticacysta* dinocysts, have been reported from presumed early Miocene (likely Burdigalian) of the Norwegian and Nordic seas [*Damassa*, 1998; *Williams and Manum*, 1999], we conclude that this "zebra" interval is Burdigalian (see *Sangiorgi et al.* [2008] for detailed discussion). This early Miocene age assessment for the subunit 1/5 is further supported by the recovery of early Miocene agglutinated foraminifera at the base of subunit 1/4 [*Kaminski*, 2007, and references therein], where samples are palynologically barren.

[10] Using the midpoint of the Burdigalian as an approximate age [see *Jakobsson et al.*, 2007; *Backman et al.*, 2008], the oldest sediments above the hiatus have been assigned an age of 18.2 Ma using the timescale of *Lourens et al.* [2005].

### 2.2. Palynology

[11] Seventy samples from subunits 1/6, 1/5, and 1/4 were selected for palynological analysis: These included closely spaced samples (up to 1-cm spacing) in the lower part of subunit 1/5, the banded "zebra" interval, and immediately below the hiatus (Figure 1). For dinocyst and other nonterrestrial palynomorph analysis, samples were processed without oxidation, as outlined by *Wood et al.* [1996]. Processing of terrestrial palynomorphs (pollen and spores) included oxidation with 35% $HNO_3$ and staining with Bismarck Brown. All palynomorphs assemblages were counted using a light microscope at a magnification of 400X. When possible, dinocysts were identified to species level, and pollen and spores were identified to genus or family level. Other palynomorphs (acritarchs, freshwater algae/algal remains such as *Pediastrum*, *Tasmanites*, *Botryococcus*, *Cymatiosphaera* spp., and fungal spores) and foraminifer linings were also counted. Total dinocyst percentages are calculated relative to the total palynomorphs. Dinocyst percentages are calculated on the total dinocysts counted. Reworked dinocysts are not included in the total dinocyst counts. We also determined dinocyst, pollen, spores, and palynomorph concentrations (e.g., dinocysts/gram dry sediment).

### 2.3. Siliceous Microfossils

[12] Biogenic silica is poorly preserved in the ACEX sediments above 202.10 mcd in subunit 1/6, and siliceous microfossils occur rarely within the "zebra" interval. Methods and results for siliceous microfossil analysis for subunit 1/6 are provided by *Stickley et al.* [2008]. An additional eight samples through cores M0002A-46X and M0002A-45X in subunits 1/6 and 1/5 (Figure 2)

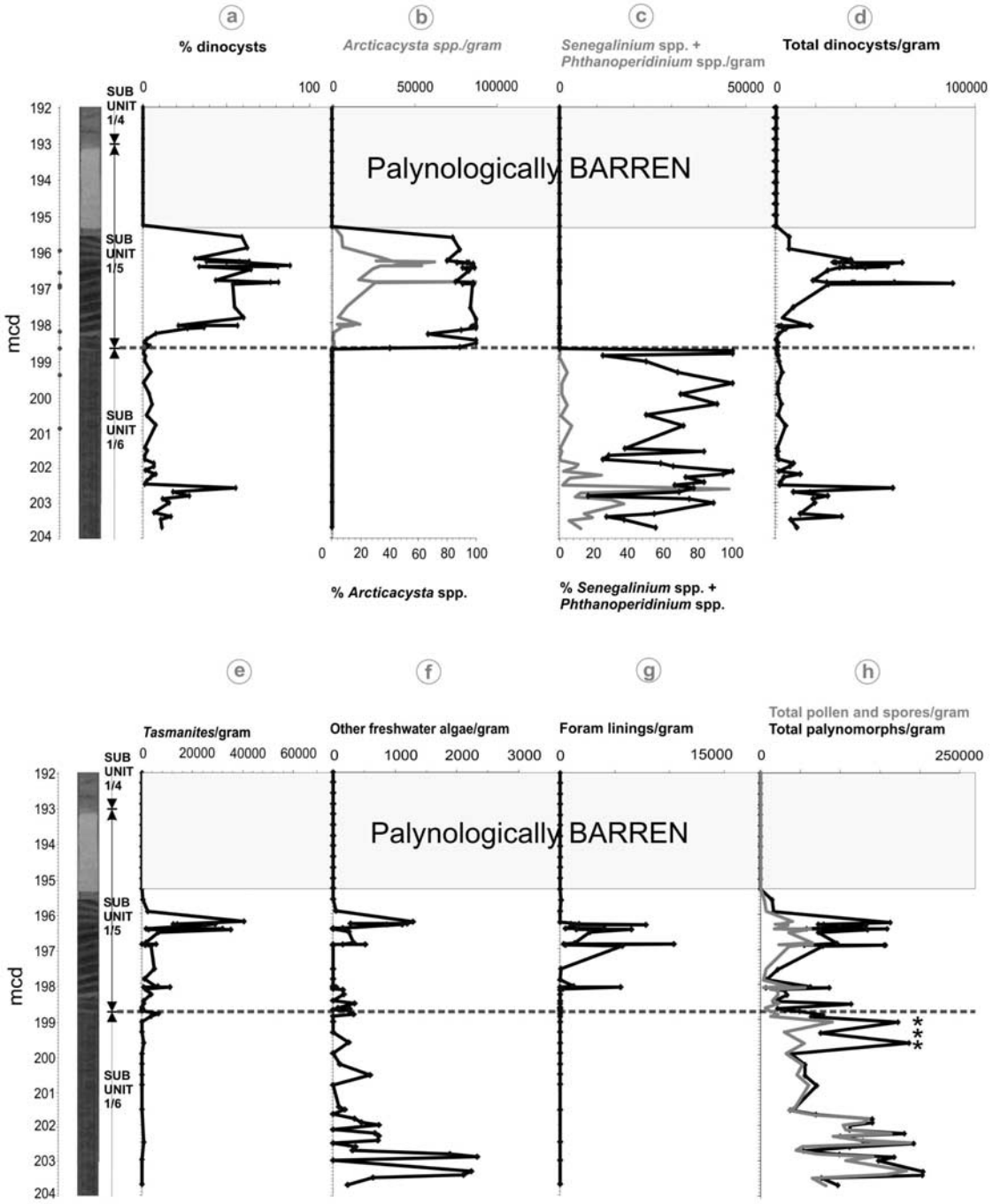


**Figure 2.** Percentages and concentrations of the most represented palynomorphs and foraminifer linings in the ACEX section studied (cores 2A 47X 3W to 2A 44X 1W, 203.70–191.99 mcd). Palynologically barren interval is indicated. Dashed line represents the position of the hiatus at 198.70 mcd. Gray dots on the depth (mcd) axis indicate samples where siliceous microfossils have been found (see text). Asterisks indicate the position of the three samples where abundant fungal spores have been found.

were analyzed to evaluate siliceous microfossil content, previously reported as ''rare'' (diatoms only) and only in the core-catcher of core M0002A-46X [*Expedition 302 Scientists*, 2006]. Silica-selective processing and analytical techniques follow those outlined by *Stickley et al.* [2008].

[13] The five major siliceous microfossil groups present in the ACEX sediments are diatoms, chrysophyte cysts, ebridians, silicoflagellates, and siliceous endoskeletal dinoflagellates (e.g., actiniscidians). All of these groups except actiniscidians were encountered in the eight samples from cores M0002A-45X and M0002A-46X. The diatoms and the ebridians were classified as brackish marine, and the chrysophyte cysts as mostly freshwater, indicators [*Stickley et al.*, 2008]. *Stickley et al.* [2008] also consider the

chrysophyte cysts as likely having lived and encysted "in situ" in the central Arctic surface waters as opposed to being transported by river runoff.

### 2.4. Inorganic Geochemistry

[14] Quantitative X-ray fluorescence (XRF) measurements were performed on freeze-dried and homogenized (agate ball mill) sample powders. Six hundred mg of sample were mixed with 3600 mg of a mixture of dilithiumtetraborate/lithiummetaborate (50% $Li_2B_4O_7$/50% $LiBO_2$), preoxidized at 500°C with $NH_4NO_3$ (p.a.), and fused to glass beads. These were analyzed for major and minor elements using a Philips PW 2400 X-ray spectrometer. Analytical precision and accuracy were better than 5% for all elements, as checked by in-house and international reference rocks. Total sulfur (TS) was determined using an Eltra CS 500 IR analyzer. Precision and accuracy of TS analyses were better than 3%.

[15] Selected trace metals (TM), including Rare Earth Elements (REE), were analyzed by an "Element 2" ICP-MS (Finnigan MAT, Germany). For acid digestions, 50 mg of sample were preoxidized with 2 mL $HNO_3$ (65%) in polytetrafluoroethylene (PTFE) vessels overnight and then heated with 3 mL HF (40%) and 3 mL $HClO_4$ (70%) in closed PTFE autoclaves (PDS-6) for 6 h at 180°C. After evaporation on hot plates at 180°C to incipient dryness, four times 3 mL 6N HCl aliquots were added and evaporated again. The wet residue was dissolved in 1 mL $HNO_3$ (65%) and diluted to 10 mL with deionized water and heated once again in closed PTFE autoclaves (PDS-6) for 2 h at 180°C. The acid digestions were diluted to 50 mL, and one drop of HF was added for stabilization of Light Rare Earth Elements (LREE). $HNO_3$, HCl, and $HClO_4$ were purified by subboiling distillation. HF of Suprapure® (Merck) quality was used. Prior to analysis the clear solutions were diluted 1:5 with 2% v/v $HNO_3$. Analytical precision was better than 8% (for detailed information, see *Schnetger* [1997]). Procedures and accuracy of all methods were checked with international and in-house reference materials.

### 2.5. Glycerol Dibiphytanyl Glycerol Tetraethers Analysis: $TEX_{86}$ and BIT Index

[16] Sediments (2–4 g dry weight) were processed following the methodology described by *Schouten et al.* [2007]. HPLC/MS analyses were performed according to *Hopmans et al.* [2000, 2004] and *Schouten et al.* [2007]. Glycerol Dibiphytanyl Glycerol Tetraethers (GDGTs) were detected by Single Ion Monitoring (SIM) of their $(M + H)^+$ ions (dwell time = 234 ms) and quantified by integration of the peak areas. The Tetra Ether Index of lipids with 86 carbon atoms ($TEX_{86}$) was calculated according to *Schouten et al.* [2002] and converted to temperatures using these authors' equation:

$$TEX_{86} = 0.015T + 0.28 \quad (1)$$

[17] The Branched and Isoprenoid Tetraether (BIT) index was calculated according to *Hopmans et al.* [2004]. Replicate analysis of samples shows that the reproducibility was 0.7°C in $TEX_{86}$ and ±0.01 in the BIT index.

## 3. Results

### 3.1. Palynology

[18] Subunit 1/6 is characterized by high concentrations of terrestrial palynomorphs (pollen and spores, Figure 2h), particularly between 203.70 and 201.57 mcd, where terrestrial palynomorphs are more abundant than in the upper part of subunit 1/6 or lower subunit 1/5. Likewise, dinocysts in subunit 1/6 are most abundant in the interval between 203.70 and 201.91 mcd.

[19] Freshwater algae (*Pediastrum*, *Botryococcus*, *Tasmanites*, *Cymatiosphaera* spp.) are present in varying abundance in subunit 1/6 and lower subunits 1/5 (Figures 2e and 2f). Massulae of the freshwater fern *Azolla* were found between 203.49 and 202 mcd. *Tasmanites* are mostly restricted to subunit 1/5, with peak abundance at 196.45–196.23 mcd (Figure 2e).

[20] In the lower part of subunit 1/5 (198.70–195.30 mcd), the "zebra" interval, dinocysts and pollen are fairly well preserved, and dinocysts usually are abundant. Although pollen typically is abundant in this interval, the lowest concentrations occur at and directly above the hiatus (Figure 2h). Dinocyst preservation is also poor in this interval, and one sample below the hiatus (at 198.72 mcd) contains no dinocysts.

[21] The interval between 195.30 and 191.99 mcd (upper subunit 1/5 and lower subunit 1/4) is almost completely barren of palynomorphs, with only sparse bisaccate pollen grains. We therefore considered this interval to be palynologically barren (Figures 1, 2, and 3).

#### 3.1.1. Dinocysts

[22] Dinocyst percentages and concentrations are highest in the lower part of subunit 1/6 (203.70 to 202.60 mcd) and in subunit 1/5 above 198.17 mcd (Figures 2a and 2d). In subunit 1/6 (from 203.70–198.70 mcd) the dominant dinocysts taxa are *Senegalinium* spp. and the *Phthanoperidinium* spp. They represent 20–100% of the dinocyst assemblages, with the highest concentrations between 203.70 and 201.91 mcd (Figure 2c). Other common dinocysts in subunit 1/6 are *Cribroperidinium* sp. and *Leptodinium* sp., with rare *Cordosphaeridium fibrospinosum, Homotryblium* sp., *Lentinia* sp., and *Lejenecysta* sp. (e.g., one or two specimens per slides in some of the samples).

[23] An outstanding feature of the record is the palynological change across the hiatus (below and above 198.70 mcd). Although the number of dinocyst species is uniformly low in the interval analyzed, in contrast to much more diverse assemblages from the Norwegian-Greenland seas in coeval intervals [e.g., *Firth*, 1996; *Eldrett et al.*, 2004], the hiatus is marked by a striking shift in the dinocyst dominance. Above the hiatus (198.70 to 195.30 mcd), the lower part of subunit 1/5, the "zebra" interval, is marked by the sudden appearance and the dominance of *Arcticacysta* (*A. backmanii* and *A. moraniae*) dinocysts [*Sangiorgi et al.*, 2008] (Figure 1). *Arcticacysta* comprises between 40 and 100% of assemb-

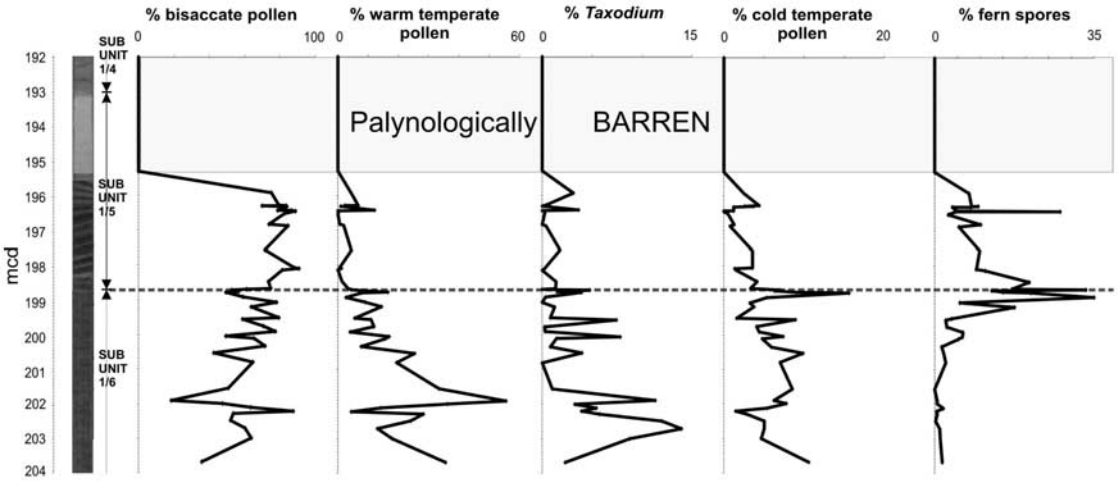


**Figure 3.** Percentages of the main pollen and spore groups (see text) in the ACEX section studied (cores 2A 47X 3W to 2A 44X 1W, 203.70–191.99 mcd) with indication of the palynologically barren interval. Dashed line indicates the position of the hiatus at 198.70 mcd.

lages, and its concentration is as high as 87,000 cysts/gram dry sediment (Figure 2b).

#### 3.1.2. Pollen and Spore Assemblages

[24] Pollen and spore concentrations are also high between 203.70 and 201.57 mcd in subunit 1/6, ranging up to 180,000 grains/g dry sediment (Figure 2h). The interval is characterized by the dominance of bisaccate grains (more *Picea* (spruce) than *Pinus* (pine)), abundant warm temperate species (i.e., *Quercus* (oak), *Juglans* (walnut), and *Ulmus* (elm)), and common occurrence of pollen of *Taxodium* (cypress) and cool temperate species (*Betula* (birch), *Alnus* (alder), and *Tsuga* (hemlock)) (Figure 3).

[25] In the upper part of subunit 1/6 (201.57–198.70 mcd), warm temperate species and *Taxodium* pollen are less abundant, and bisaccate pollen dominates assemblages. Fern spore abundance increases progressively throughout this interval, comprising 13–35% of assemblages between 198.92 and 198.70 mcd (Figure 3). The three uppermost samples in this interval are characterized by abundant masses of fungal spores (Figure 2h).

[26] Pollen assemblages of subunit 1/5 between the hiatus at 198.70 mcd and the palynologically barren zone at 195.30 mcd are dominated strongly by bisaccate pollen, which comprises >70% of assemblages. Among the bisaccate grains in this unit, *Pinus* pollen is more abundant than *Picea* pollen. Warm and cool temperate species each typically comprise <5% of assemblages, and fern spore abundance is variable, ranging from 3–28% of assemblages.

### 3.2. Agglutinated Benthic Foraminifers

[27] Fluctuating but fairly abundant concentrations of organic remains of agglutinated benthic foraminifers were found in the "zebra" interval, between 198.14 and 195.60 mcd (Figure 2g). They include cosmopolitan *Cyclammina pusilla*, *Cyclammina cancellata*, and *Ammolagena clavata* (M. Kaminski, personal communication).

### 3.3. Siliceous Microfossils

[28] Siliceous microfossils are abundant in the interval ~203.4–202.5 mcd (up to $\sim 2 \times 10^8$ total silicofossil specimens per gram [see *Stickley et al.*, 2008]) (Figures 2 and 4d), with chrysophyte cysts the most abundant group, followed by ebridians and then diatoms, which have a low diversity [*Stickley et al.*, 2008].

[29] Above 202.1 mcd, biogenic silica is almost absent except for some exceptionally rare occurrences (e.g., one specimen per slide or approximately <60 total silicofossil specimens per gram) in cores M0002A-45X and M0002A-46X (~201–196 mcd) (Figure 4d). These are rare specimens of the ebridian *Pseudammodochium dictyoides*, the diatom *Anaulus arcticus*, species of the diatom genera *Hemiaulus*, *Stephanopyxis*, *Odontotropis* and *Pyxilla,* rare "needle-like diatoms" [see *Stickley et al.*, 2008], rare silicoflagellates, and one chrysophyte cyst specimen at 196.53 mcd. We assume all of these siliceous microfossils are reworked from unit 2, the biosiliceous ooze, where they are abundant and stratigraphically consistent [*Stickley et al.*, 2008]. Occurring alongside these reworked specimens are siliceous microfossils we consider to be "in situ": a heavily silicified bowl-shaped siliceous microfossil (>100 $\mu$m) of unknown affinity occurring in comparative abundance and only within one sample at 196.53 mcd plus very rare occurrences (two or three specimens per slide) of small *Thalassiosira* spp. and *Denticula* spp., suggestive of a

**Figure 4.** Inorganic geochemistry proxies in the ACEX section studied (cores 2A 47X 3W to 2A 44X 1W, 203.50–191.99 mcd). Dashed line indicates the position of the hiatus at 198.70 mcd. Gray dots on the depth (mcd) axis of the Si/Al graph indicate samples where siliceous microfossils have been found (see text). In this graph, rare occurrence of siliceous microfossils and high occurrence of biosilica (light gray rectangle) are indicated.

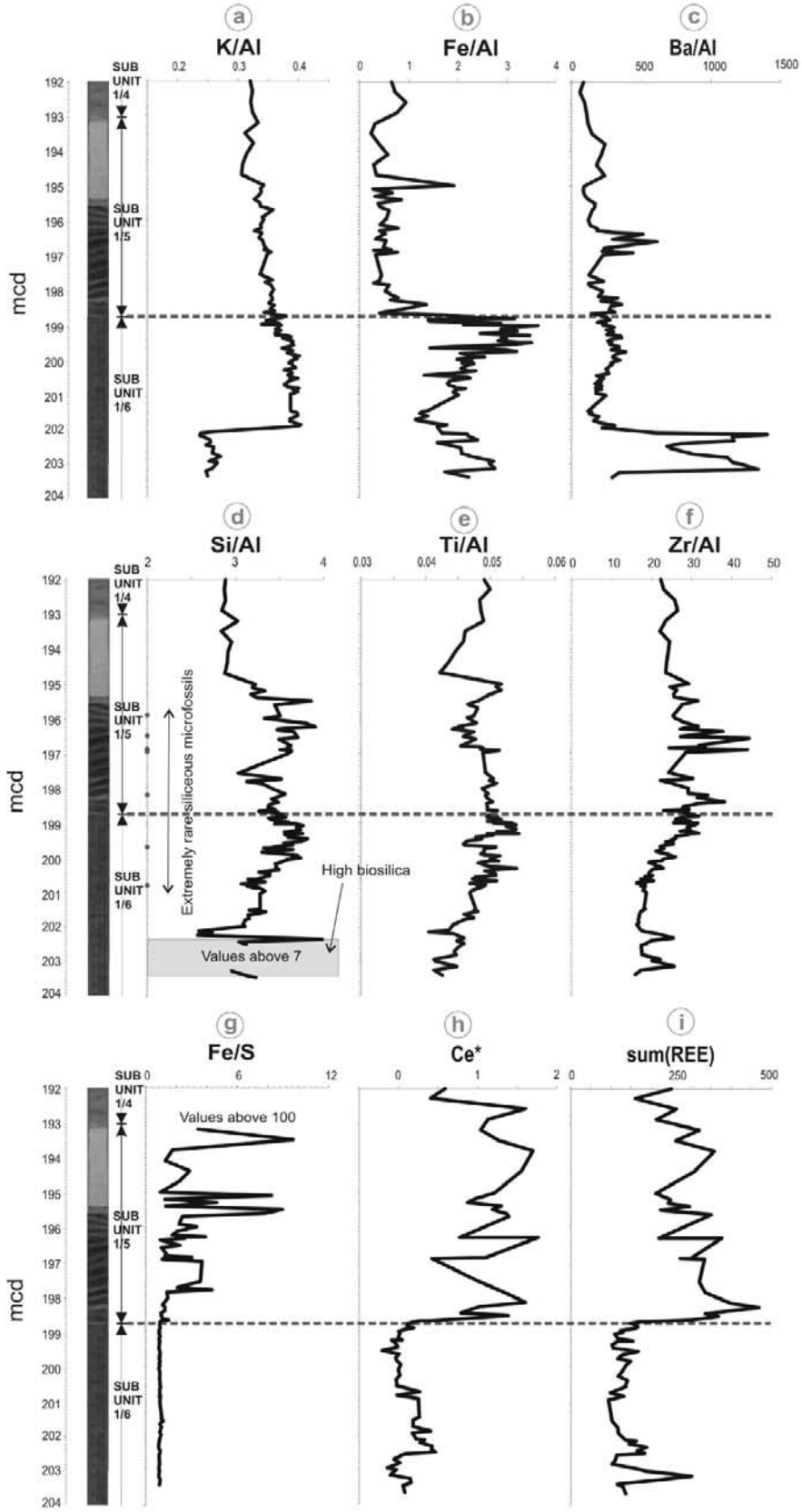
a
K/Al
b
Fe/Al
c
Ba/Al
d
Si/Al
e
Ti/Al
f
Zr/Al
g
Fe/S
h
Ce*
i
sum(REE)
SUB UNIT 1/4
SUB UNIT 1/5
SUB UNIT 1/6
mcd
Extremely rare siliceous microfossils
High biosilica
Values above 7
Values above 100

**Figure 4**

**Table 1.** Element Enrichment in Dark Versus Light Layers of the "Zebra" Interval[a]

| Element | Average Light Layer | Average Dark Layer | EF Dark Layer | Element | Average Light Layer | Average Dark Layer | EF Dark Layer |
|---|---|---|---|---|---|---|---|
| TS, % | 1.34 | 3.65 | 2.7 | Re/Al* | 0.019 | 0.081 | 4.3 |
| TOC, % | 3.23 | 7.16 | 2.2 | Mo/Al* | 3.1 | 10.3 | 3.3 |
| Fe/Al | 0.38 | 0.66 | 1.7 | As/Al* | 3.1 | 9.6 | 3.1 |
| P/Al | 63 | 84 | 1.3 | Co/Al* | 3.2 | 8.4 | 2.6 |
| Mg/Al | 0.156 | 0.167 | 1.1 | Zr/Al* | 26.4 | 32.1 | 1.2 |
| K/Al | 0.289 | 0.294 | 1.0 | Sr/Al* | 17.7 | 20.0 | 1.1 |
| Si/Al | 3.49 | 3.54 | 1.0 | U/Al* | 2.84 | 3.15 | 1.1 |
| Ti/Al | 0.048 | 0.048 | 1.0 | Rb/Al* | 12.1 | 12.5 | 1.0 |

[a]Element ratios are weight ratios. Asterisk indicates value multiplied by $10^{-4}$. EF = enrichment factor.

"no older than Oligocene" age, if these are similar to those reported from the Norwegian Sea [*Schrader and Fenner*, 1976; *Dzinoridze et al.*, 1978]. A comparative scanning electron microscope–based study of the *Thalassiosira* and *Denticula* Norwegian Sea specimens and those of the Lomonosov Ridge is required before this assumption can be verified.

### 3.4. Inorganic Geochemistry

[30] The interval from 203.5 to 192 mcd is characterized by large shifts in geochemical composition. At around 202 mcd a very marked increase in K/Al ratio from 0.21 to 0.35 occurs within a 2-samples interval, 16 cm apart (202.12 and 201.96 mcd), indicating a drastic change in sediment provenance (Figure 4a).

[31] Below this interval is a prominent diagenetic front (from 203.3–202 mcd), generally Si-rich because of abundant siliceous microfossils (Figure 4d), that provides the pore space required for diagenetic mineral formation. This interval is also enriched in Ba/Al (most likely barite) (Figure 4c), mobilized during diagenesis.

[32] Above the K/Al shift from ~202 to 198.70 mcd is a pyrite-rich interval, as indicated by very high Fe/Al (Figure 4b), and S/Al (not shown). Another feature of the interval above the 202 mcd lithological break is the steady increase in Zr/Al, Ti/Al, and Si/Al ratios (disregarding the Si-rich section below 202 mcd) (Figures 4d, 4e, and 4f). This geochemical signal points toward increased current velocities and/or a shallower environment, because the above elements are enriched in heavy minerals or quartz [e.g., *Dellwig et al.*, 2000].

[33] Significant geochemical changes are not evident within the "zebra" interval. The white and dark layers differ in chemical composition and represent relatively more (light layers) or less (dark layers) oxidized material (see Table 1). Considerable enrichments are seen in the bulk parameters of the major elements such as total sulfur (TS), total organic carbon (TOC), Fe, and to a slightly lesser extent P and the trace metals (TM) Re, Mo, As, and Co (in decreasing order). By contrast the lithogenic elements Mg, K, Si, Ti, Zr, Sr, Rb, and even the redox sensitive element U show no enrichment. From the hiatus at 198.70 mcd to 195 mcd, diagenesis has caused major alterations. A truly oxic environment, comparable to that of today, characterizes sediments only above 195 mcd.

[34] The geochemical data indicate a potential placement for a hiatus at either 202 mcd (K/Al break) or at 198.70 mcd (shift in Fe/Al ratio). However, changes in the enrichment of Rare Earth Elements (REE) (Figure 4i) and in the Cerium (Ce)- anomalies (Figure 4h) indicate that 198.70 mcd is the correct position for a hiatus. None of the samples below the hiatus exhibit a distinctive positive Ce-anomaly, but there is a drastic change above the hiatus. Changes in the REE and in the Ce-anomaly are most likely related to an intensification of the Mn-cycle and the development of a more oxic environment.

### 3.5. $TEX_{86}$ and BIT Index

[35] Sea surface temperatures (SSTs) were reconstructed using $TEX_{86}$ [*Schouten et al.*, 2002]. The record shows three distinct intervals. Between 203.70 and 201.49 mcd, temperatures were relatively constant with an average of 8.2 ± 1.4°C (Figure 5). Temperatures were lower between 200.47 and 198.70 mcd, averaging 4.7 ± 1.0°C. The hiatus is clearly marked by a sharp change in $TEX_{86}$ temperatures, which show an initial abrupt increase from 4 to 15°C (between 198.70 and 198.56 mcd) followed by a rapid rise to relatively stable values of 19.7 ± 1.5°C. Above 195 mcd, $TEX_{86}$ was not measurable as samples were too oxidized.

[36] The BIT index, a proxy for the relative contribution of fluvially transported soil organic matter [*Hopmans et al.*, 2004], shows low values (<0.1) with no significant change below and above the hiatus (Figure 5). BIT indices are somewhat higher above 198.70 mcd and substantially increase above 195.50 mcd.

### 3.6. Paleoenvironmental Reconstructions

[37] Our multiproxy study allows the recognition of four different paleoenvironmental and paleoceanographical phases (A–D), two preceding (A and B) and two following (C and D) the hiatus at 198.70 mcd (Figure 5).

[38] Phase A: The interval between 203.70 and 201.91 mcd (Figure 5) shows the highest dinocyst concentrations within subunit 1/6 (Figure 2). Dinocysts can provide useful information on the sea surface water features, such as temperature, productivity, salinity, and presence of sea ice [e.g., *Marret and Zonneveld*, 2003; *Sluijs et al.*, 2005]. The paleoenvironmental signal derived from dinocysts indicates fresh to brackish surface waters, with *Senegalinium* spp. and *Phthanoperidinium* spp. typically dominating the assemblages. Indirect and direct evidence suggest that these genera are likely produced by dinoflagellates that tolerated low surface water

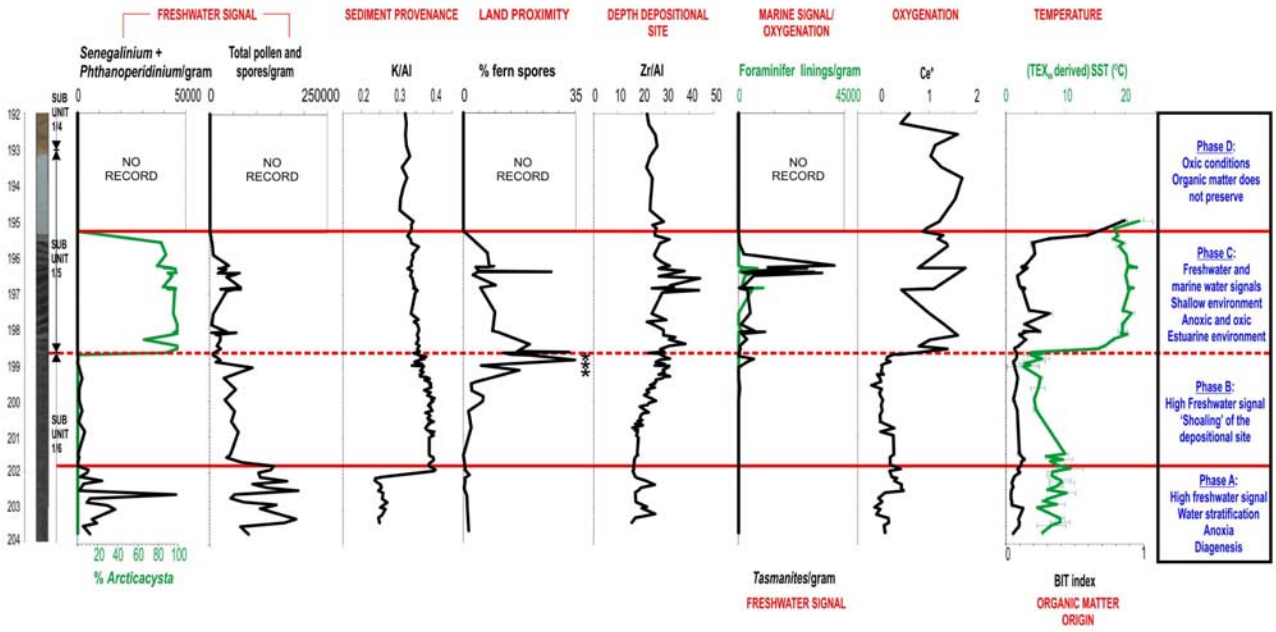


**Figure 5.** Summary diagram indicating the major paleoenvironmental changes (phases A–D), two below and two above the hiatus as derived from the multiproxy approach applied. Dashed red line indicates the position of the hiatus at 198.70 mcd. Sea surface temperatures (SSTs) as derived from the paleothermometer $TEX_{86}$ and the Branched and Isoprenoid Tetraether (BIT) index are also shown. Asterisks indicate the position of the three samples where abundant fungal spores have been found.

salinities [e.g., *Sluijs et al.*, 2003; *Brinkhuis et al.*, 2006; *Sluijs et al.*, 2006, 2008]. Abundant occurrences of these taxa are in many records accompanied by abundant terrestrial spores and pollen, as well as fossils of freshwater algae [*Sluijs et al.*, 2005]. *Senegalinium* spp. and *Phthanoperidinium* spp. comprise peridinioid species. Most of the extant peridinioids are heterotrophic, predominantly feeding on diatoms [e.g., *Jacobson and Anderson*, 1986], and their abundance is used to indicate primary productivity and prey availability. Although oversimplified, the peridinioid-productivity relation represents a valuable approach to reconstruct and estimate first-order paleoproductivity in the Paleogene (see discussion by *Sluijs et al.* [2005] and references therein). Hence we interpret phase A as being characterized by high productivity, which is supported by high diatoms abundance, high Si/Al-ratio, and inferred high deposition of biogenic silica. The high Ba/Al (Figure 4c), most likely barite, suggests that barite is partly mobilized during diagenesis, but also reflects enhanced productivity. The diagenetic front may have formed because of a drastic change in sedimentation rate or to the development of a hiatus [*Bréhéret and Brumsack*, 2000]. It can also be related to the formation of mixed carbonate minerals under euxinic conditions and sporadic flushing with oxygenated waters, comparable modern processes in deeper regions of the Baltic Sea [*Huckriede and Meischner*, 1996]. A strongly stratified water column with a fresh to brackish surface layer and more saline subsurface layers, is shown by abundant freshwater chrysophyte cysts [*Stickley et al.*, 2008] and concomitant marine ebridians and the diatom genera, *Coscinodiscus*, *Hemiaulus* and *Pyxilla*, which are known marine taxa from other Paleogene settings globally.

[39] The occurrence of massulae of the freshwater fern *Azolla* between 203.49 and 202 mcd, the high concentration of total pollen and spores (Figure 2h) and freshwater algae (Figure 2f), and abundant chrysophyte cysts [*Stickley et al.*, 2008] confirm a strong runoff signal and/or freshwater influence at the site. This contrasts with low (<0.1) BIT index values, which suggest relatively little influx of soil organic matter. Substantially elevated Fe/Al ratios (Figure 4b), well above the average shale level [*Wedepohl*, 1971], indicate a significant fluvial contribution. All available Fe is converted into pyrite as documented by a Fe/S ratio close to unity. This suggests that fluvial input provided the necessary iron [*Pokrovsky and Schott*, 2002], and seawater provided the necessary sulfate for microbial sulfate reduction to allow pyrite formation.

[40] Evidence from terrestrial palynomorphs provides information on paleoclimate and proximity to land. For example, pollen assemblages between 203.70 and 201.91 mcd indicate a pollen source from warm temperate forests (Figure 3). The present northern limit of *Taxodium* is~38°N in North America, and *Juglans* is most common south of 45°N [*Iverson et al.*, 1999]. Sea surface temperatures (SSTs) reconstructed for this interval using $TEX_{86}$are relatively warm, averaging 8.2 ± 1.4°C.

[41] In phase B, between 201.91 and 198.70 mcd (Figure 5), dinocysts are never abundant, and sometimes rare. The genera *Senegalinium* and *Phthanoperidinium*

are still dominant, again suggesting fresh to brackish surface waters. High freshwater input is confirmed by the highest Fe/Al ratios (up to 3.5, i.e., 5-fold higher than average shale) of the entire record. A progressive increase in conifer pollen and decrease in pollen of warm temperate species indicate atmospheric cooling. Likewise, $TEX_{86}$-derived SSTs show cooler conditions ($T = 4.7 \pm 1.0°C$). In the latter part of phase B (199.2 and 198.70 mcd), sharp increases in abundance of fern spores and fungal spores indicate deposition either close to shore or on land. Earlier research [*Mudie*, 1980, 1982] examining the distribution of pollen in marine sediments along the eastern Canadian coast indicates that fern spores are well-represented primarily in near-shore sites, with minimal transport offshore by currents. Combined with the abundance of fungal material, these data indicate that the depositional site was at or near sea level at this critical interval. Increasing Zr/Al and Ti/Al ratios (Figures 4 and 5) may indicate either stronger current velocities or a shallow setting [e.g., *Dellwig et al.*, 2000].

[42] Phase C: Above the hiatus, between 198.70 and 195.30 mcd (Figure 5), in the lower Miocene part of the section, dinocyst assemblages are almost monogeneric. The dominant genus is *Arcticacysta* [*Sangiorgi et al.*, 2008]. The ecological preference of the genus is unknown. However, the existence of monogeneric assemblages is suggestive of restricted environmental conditions, such as hyperstratification, euryhaline conditions or increased seasonal temperature contrast. *Arcticacysta* species are peridinioids, which may also be interpreted as indicative of high productivity. Diatoms are, however, rarely preserved, probably because of diagenetic alteration. The fluctuating but high concentrations of *Tasmanites* and other freshwater algae, particularly in the upper meter of this phase C (Figures 2e and 2f), suggest strong freshwater influence. This, coupled with the occurrence of remains of agglutinated benthic foraminifera, indicate alternating freshwater to marine conditions, and/or decoupling, at least seasonally, between an upper freshwater layer and a more saline deep water layer. The occurrence of deep water (outer neritic to upper bathyal) agglutinated foraminifers [e.g., *Kaminski*, 2007] suggests at least intermittent ventilation of bottom waters. This assumption is strongly supported by the positive Ce-anomalies in this interval, indicating an intensification of the oxidative Mn-cycle. The dominance of bisaccate pollen and the scarcity of warm temperate pollen indicate cooler climate on the surrounding land. In contrast, SSTs derived with the $TEX_{86}$ show average values of $19.7 \pm 1.5°C$. The BIT index also substantially increases in this interval. The continued presence of fern spores (~5%) suggests that the site remained near sea level, at least until conditions changed to cause the palynologically barren zone at 195.30 mcd. Finally, the presence of sparse reworked dinocysts of Cretaceous to Oligocene age [*Sangiorgi et al.*, 2008] suggests that older than Miocene sediments were deposited somewhere around the site and there later redeposited.

[43] Phase D: The palynologically barren interval above 195.30 mcd (Figure 5) points to well-oxygenated waters (even at depth), which prevented preservation of organic remains. This is confirmed by the positive Ce anomalies and high Fe/S (Figures 4g and 4h), particularly above 193 mcd. $TEX_{86}$ was not measurable in most of this interval, as samples were highly oxidized. In the two samples where $TEX_{86}$ could be calculated, SSTs are high and comparable to those found in the previous interval.

## 4. Discussion

### 4.1. Clues for the 26 Ma Hiatus

[44] Our multiproxy paleoenvironmental reconstruction of central Arctic Ocean sediments from Lomonosov Ridge provides insights into factors related to the 26 million years hiatus in the mid-Cenozoic. Below the hiatus (phase B, Figure 5), increases in the Ti/Al (Figure 4e) and Zr/Al ratios may indicate either enhanced current velocity and/or shallow environments. However, the lack of evidence for major changes in grain size and the consistently high TOC values (~4–5%) below and above the hiatus [*Expedition 302 Scientists*, 2006; *Stein et al.*, 2006] make the progressive shoaling of the Lomonosov Ridge depositional site the preferred hypothesis to explain increases in these heavy minerals. A depositional site at or near sea level is confirmed by peaks in fern spores and the occurrence of fungal spores just below the hiatus. Fern spores are most common in near-shore sites, with minimal transport offshore by currents [e.g., *Mudie*, 1980, 1982]. Above the hiatus (phase C), sediments were also deposited in a site very close to or at sea level (see abundance of fern spores). The sparse reworking of dinocysts in this phase [*Expedition 302 Scientists*, 2006; *Sangiorgi et al.*, 2008] is a clear indication that older sediments were deposited somewhere around the site and were there later redeposited. Consequently, the missing sediment record can be explained by erosion and/or nondeposition of sediments in a site, which remained close to or at sea level for several million years. When the Lomonosov Ridge started subsiding, older sediments were washed into the drill site. The interaction of sea level changes and tectonic activity (possibly uplift) must be invoked as possible causes for such a long gap in the sediment record.

[45] A shallow water setting for the Lomonosov Ridge in the mid-Cenozoic is certainly inconsistent with classical postrifting thermal subsidence models for passive margins [*McKenzie*, 1978] as well as the published model describing the subsidence of the ridge on the basis of similar "thermal cooling" assumptions and derived through modifications of empirical observations on the subsidence of newly formed oceanic crust [*Moore et al.*, 2006].

[46] Reconciling the shallow water setting ultimately depends on the mechanism invoked to explain the anomalous subsidence pattern for this segment of the Lomonosov Ridge. There is ample evidence for either Cenozoic uplift or rapid Neogene subsidence on many of the passive margins that surround the North Atlantic and Arctic Oceans [*Cloetingh et al.*, 1990; *Eyles*, 1996; *Rohrman and van der Beek*, 1996] with episodes of mid-Cenozoic uplift well documented in both the Norwegian-Greenland seas [*Rohrman and van der Beek*, 1996, *Tsikalas et al.*, 2005] and in western Greenland [*Japsen et al.*, 2006].

[47] Although it remains unclear whether the Lomonosov Ridge was uplifted following a period of postrifting subsidence, remained near sea level until the Miocene, or subsided and was subsequently unroofed during large basin-wide fluctuations in regional sea level, the paleoenvironmental data surrounding the hiatus is unambiguous in its assignment of a shallow water setting during the mid-Cenozoic and should be used to correct and guide subsidence modeling of the Lomonosov Ridge.

### 4.2. Paleoenvironment: Arctic Ocean From a "Lake" to a "Marine" Phase

[48] We have also documented the different environments associated with important paleoceanographic changes, which track the evolution of the Arctic Ocean from its "lake" phase in the Eocene to its "estuarine" and fully marine phases in the early Miocene following the opening of the Fram Strait [see also *Jakobsson et al.*, 2007].

[49] Sediments below the hiatus (phases A and B, Figure 5) indicate an environment primarily dominated by fresh to brackish surface waters, where high water stratification prevailed. Fresh surface waters have characterized most of the Paleogene in the Arctic Ocean, with greatest intensity reached at the *Azolla* interval around ~49 Ma [e.g., *Expedition 302 Scientists*, 2006; *Brinkhuis et al.*, 2006]. The combined effect of Eocene Arctic Ocean paleogeography with no deep connections to the oceans [e.g., *Brinkhuis et al.*, 2006; *Jakobsson et al.*, 2007], the relatively warm Eocene temperature with mild winters [*Greenwood and Wing*, 1995], and the humidity estimate about twice that of today for the higher northern latitudes (80°N) [*Jahren and Sternberg*, 2003] all indicate that surface water was strongly affected by freshwater input through high river runoff and/or high precipitation. Our data indeed indicate a warm middle Eocene environment ($TEX_{86}$-derived SSTs ~8°C), with values fully comparable to previously published high-latitude (~80°N) continental middle Eocene temperature estimates (e.g., 8.2–9.3°C from Axel Heiberg Island and Ellesmere) [*Greenwood and Wing*, 1995]. They are slightly lower than those for the early middle Eocene Arctic Ocean during the *Azolla* event (SSTs = 10–13°C) [*Brinkhuis et al.*, 2006] and the late early to early middle Eocene in the northern continental United States (MAT = 10–15°C) [*Greenwood et al.*, 2005].

[50] A sharp shift in sediment provenance (K/Al) followed by a decrease in land (pollen) and sea water temperatures ($TEX_{86}$-derived SSTs ~5°C) characterize the sediments leading to the hiatus. This cooling of about 3°C could mirror the global Eocene cooling trend [e.g., *Zachos et al.*, 2001]. Phases A and B represent the "lake" phase of the Arctic Ocean [see *Jakobsson et al.*, 2007].

[51] Sediments above the hiatus (phase C, Figure 5) in the "zebra" interval contain dominant early Miocene (Burdigalian) *Arcticacysta* dinocysts [see also *Sangiorgi et al.*, 2008]. The almost monogeneric dinoflagellate assemblage indicates a restricted environment. The concomitant influence of freshwater (high number of remains of freshwater algae) and marine waters (foraminifer linings) and the alternation between oxic and anoxic conditions indicate the transitional "estuarine" phase of the Arctic Ocean preceding the full opening of the Fram Strait in the early Miocene [*Jakobsson et al.*, 2007]. The (outer neritic to upper bathyal) foraminifer species found in our record are the same as those found in early Miocene sediments in ODP Hole 909C in the Fram Strait and in the Norwegian-Greenland seas [*Kaminski et al.*, 2006; *Kaminski*, 2007]. This suggests a deeper connection to the North Atlantic.

[52] It is difficult to explain the contrasting temperature signal obtained for this interval, with colder conditions on land (based on pollen) and $TEX_{86}$-derived SSTs of ~15–19°C (Figure 5), extremely high for an "icehouse" Arctic Ocean. Although MATs above 20°C have been reconstructed for the Miocene Climatic Optimum in central Europe at latitudes of about 45°N [*Bohme*, 2003; *Mosbrugger et al.*, 2005], our values seem interestingly high, i.e., comparable to the warmest late Paleocene [*Sluijs et al.*, 2006]. BIT indices (Figure 5) remain low during this interval, and thus the imprint of potentially transported terrestrial tetraether lipids cannot be the cause of such high temperatures. Potentially, the increased oxygenation of the water column could have caused a diagenetic imprint on the $TEX_{86}$ [*Huguet*, 2007], or the tetraether lipids are of allochthonous (lower latitudes) origin. Phase C does however represent the first step of the opening of the Fram Strait [*Jakobsson et al.*, 2007]. Ingression of warmer Atlantic waters (proto–Gulf Current), possibly in a global climatic optimum scenario (Miocene Climatic Optimum), may have favored an increase in the SSTs in the Arctic Ocean during its "estuarine" phase. Further studies are needed to constrain the causes for these apparent unusually high $TEX_{86}$ (SST) values. However, present-day summer SSTs in southern Baltic and Barents seas are comparable with our $TEX_{86}$-SST values. This would imply that $TEX_{86}$-based SSTs are summer instead of mean annual temperatures and that the Arctic Ocean was warmer than expected during part of the Miocene.

[53] The absence of palynomorphs, and the extreme oxic conditions indicated by the inorganic and organic geochemistry characterizing phase D bare proves that, at this stage in the early Miocene, the Fram Strait opened and deepened enough to favor complete ventilation of the Arctic Ocean [see *Jakobsson et al.*, 2007]. At the base of this phase, $TEX_{86}$-SST values and BIT index are both very high. In highly oxidized environments, however, the signals could be biased, and BIT values can dramatically increase during prolonged oxic degradation because terrestrial organic matter tends to be preserved best [*Huguet*, 2007].

## 5. Concluding Remarks

[54] The Cenozoic sediment record recovered from the Lomonosov Ridge during Integrated Ocean Drilling Program (IODP) Expedition 302 revealed an unexpected 26 Ma hiatus between the middle Eocene and the early Miocene. Our multiproxy study of the sediments encompassing the hiatus shows a shallow water environment both below and above the hiatus. The sparse

reworking of Cretaceous to Oligocene dinocysts in the interval immediately above the hiatus [*Expedition 302 Scientists*, 2006; *Sangiorgi et al.*, 2008] is a clear indication that older sediments were deposited somewhere around the site and there later redeposited. Consequently, the missing sediment record can be explained by erosion and/or non deposition of sediments in a site, which remained close to or at sea level for several million years. Once the Lomonosov Ridge started subsiding, older sediments were washed into the drill site. A combination of sea level changes and tectonic activity (possibly uplift) are the likely caused for such a long gap in the sediment record. This sharply contrasts with the classical subsidence model for passive margins [*McKenzie*, 1978] as well as with the published model describing the subsidence of the ridge on the basis of "thermal cooling" assumptions [*Moore et al.*, 2006].

[55] **Acknowledgments.** This research used samples and data provided by the Integrated Ocean Drilling Program (IODP). We acknowledge Jan Backman, Martin Jakobsson, Kate Moran, Heiko Pälike, and David Spofforth for useful discussions. We thank Walter Hale (IODP Bremen core repository) for core handling. FS thanks M. Kaminski for information concerning agglutinated foraminifera and N. Welters, E. Hopmans, C. Blaga, E. van Bentum, and T. Sheehan for technical support. Netherland Organization for Scientific Research (NWO) is thanked for funding to FS, SS, JDS, and HB. The Earth Surface Dynamics Program of the U.S. Geological Survey provided funding for DW. HJB gratefully acknowledges funding through DFG grant BR 774/20 within SPP IODP/ICDP. He further thanks C. Lehner, E. Gründkens, and M. Wagner for performing the chemical analyses. CES acknowledge VISTA (Norwegian Academy of Science and Letters and Statoil) project 6248 and the Research Council of Norway (RCN). We acknowledge Ian Harding and an anonymous reviewer for constructive suggestions. This is NSG publication 20080101.

## References

Backman, J., et al. (2008), Age model and core-seismic integration for the Cenozoic Arctic Coring Expedition sediments from the Lomonosov Ridge, *Paleoceanography*, doi:10.1029/2007PA001476, in press.

Bohme, M. (2003), The Miocene Climatic Optimum: Evidence from ectothermic vertebrates of central Europe, *Palaeogeogr. Palaeoclimatol. Palaeoecol.*, *195*, 389–401.

Bréhéret, J. G., and H. J. Brumsack (2000), Barite concretions as evidence of pauses in sedimentation in the Marnes Bleues Formation of the Vocontian Basin (SE France), *Sediment Geol.*, *130*, 205–228.

Brinkhuis, H., et al. (2006), Episodic fresh surface water in the Eocene Arctic Ocean, *Nature*, *441*, 606–609.

Cande, S. C., and D. V. Kent (1995), Revised calibration of the geomagnetic polarity timescale for the Late Cretaceous and Cenozoic, *J. Geophys. Res.*, *100*, 6093–6095.

Cloetingh, S., F. M. Gradstein, H. Kooi, A. C. Grant, and M. Kaminski (1990), Plate reorganization: A cause of rapid late Neogene subsidence and sedimentation around the North Altantic?, *J. Geol. Soc. London*, *147*, 495–506.

Damassa, S. P. (1998), A Hole-Y alliance: Calciodinelloidean archeopyles in dinosporin cysts, *Palynology*, *22*, 238.

Dellwig, O., J. Hinrichs, A. Hild, and H. J. Brumsack (2000), Changing sedimentation in tidal flat sediments of the southern North Sea from the Holocene to the present: A geochemical approach, *J. Sea Res.*, *44*, 195–208.

Dzinoridze, R. N., A. P. Jousé, G. S. Koroleva-Golikova, G. E. Kozlova, G. S. Nagaeva, M. G. Petrushevskaya, and N. I. Strelnikova (1978), Diatom and radiolarian Cenozoic stratigraphy, Norwegian Basin: DSDP Leg 38, *Initial Rep. Deep Sea Drill. Proj.*, *38, 39, 40, 41*, 289–427.

Eldrett, J. S., I. C. Harding, J. V. Firth, and A. P. Roberts (2004), Magnetostratigraphic calibration of Eocene–Oligocene dinoflagellate cyst biostratigraphy from the Norwegian-Greenland Sea, *Mar. Geol.*, *204*, 91–127.

Expedition 302 Scientists (2006), Sites M0001–M0004, in Proc. IODP, vol. 302, J. Backman et al., Integr. Ocean Drill. Program Manage. Int. Inc., Edinburgh, doi:10.2204/iodp.proc.302.104.2006.

Eyles, N. (1996), Passive margin uplift around the North Atlantic region and its role in Northern Hemisphere late Cenozoic glaciation, *Geology*, *24*, 103–106.

Firth, J. V. (1996), Upper middle Eocene to Oligocene dinoflagellate biostratigraphy and assemblage variations in Hole 913B, Greenland Sea, *Proc. Ocean Drill. Program Sci. Results*, *151*, 203–242.

Greenwood, D. R., and S. L. Wing (1995), Eocene continental climates and latitudinal temperature gradients, *Geology*, *23*, 1044–1048.

Greenwood, D. R., S. B. Archibald, R. W. Mathewes, and P. T. Moss (2005), Fossil biotas from the Okanagan Highlands, southern British Columbia and northeastern Washington State: Climates and ecosystems across an Eocene landscape, *Can. J. Earth Sci.*, *42*, 167–185.

Hopmans, E. C., S. Schouten, R. D. Pancost, M. J. T. van der Meer, and J. S. Sinninghe Damsté (2000), Analysis of intact tetraether lipids in archaeal cell material and sediments using high performance liquid chromatography/atmospheric pressure ionization mass spectrometry, *Rapid Commun. Mass Spectrom.*, *14, 585–589.*

Hopmans, E. C., J. W. H. Weijers, E. Schefuß, L. Herfort, J. S. Sinninghe Damsté, and S. Schouten (2004), A novel proxy for terrestrial organic matter in sediments based on branched and isoprenoid tetraether lipids, *Earth Planet. Sci. Lett.*, *224*, 107–116.

Huckriede, H., and D. Meischner (1996), Origin and environment of manganese-rich sediments within black-shale basins, *Geochim. Cosmochim. Acta*, *60*, 1399–1413.

Huguet, C. (2007), $TEX_{86}$ paleothermometry: Proxy validation and application in marine sediments, Ph.D. thesis, Univ. of Utrecht, Utrecht.

Iverson, L. R., A. M. Prasad, B. J. Hale, and E. K. Sutherland (1999), Atlas of current and potential future distributions of common trees of the eastern United States, *Gen. Tech. Rep. NE-265*, 245 pp., Northeast. Res. Sta., U.S. For. Serv., Dept. of Agricul., Newtown Square, Pa.

Jacobson, D. M., and D. M. Anderson (1986), Thecate heterotrophic dinoflagellates: Feeding behaviour and mechanics, *J. Phycol.*, *22*, 249–258.

Jahren, A. H., and L. S. L. Sternberg (2003), Humidity estimate for the middle Eocene Arctic rain forest, *Geology*, *31*(5), 463–466.

Jakobsson, M., et al. (2007), The early Miocene onset of a ventilated circulation regime in the Arctic Ocean, *Nature*, *447*, 986–990.

Japsen, P., J. M. Bonow, P. F. Green, J. A. Chalmers, and K. Lidmar-Bergstrom (2006), Elevated, passive continental margins: Long-term highs or Neogene uplifts? New evidence from west Greenland, *Earth Planet. Sci. Lett.*, *248*, 330–339.

Kaminski, M. A. (2007), Faunal constraints for the timing of the Fram Strait opening: The record of Miocene deep-water agglutinated foraminifera from IODP Hole M0002A, Lomonosov Ridge, *IODP UK Newsl.*, *32*, 18–20.

Kaminski, M. A., L. Silye, and S. Kender (2006), Miocene deep-water agglutinated foraminifera from ODP Hole 909c: Implications for the paleoceanography of the Fram Strait Area, Greenland Sea, *Micropaleontology*, *51*, 373–403.

Lourens, L. J., F. J. Hilgen, N. J. Shackleton, J. Laskar, and D. Wilson (2005), The Neogene Period, in *A Geological Time Scale 2004*, edited by F. M. Gradstein et al., pp. 409–440, Cambridge Univ. Press, Cambridge.

Marret, F., and K. F. Zonneveld (2003), Atlas of modern organic-walled dinoflagellate cyst distribution, *Rev. Palaeobot. Palynol.*, *125*, 1–200.

McKenzie, D. P. (1978), Some remarks on the development of sedimentary basins, *Earth Planet. Sci. Lett.*, *40*, 25–32.

Moore, T. C., et al. (2006), Sedimentation and subsidence history of the Lomonosov Ridge, in *Proceedings of the Integrated Ocean Drilling Program*, vol. 302, edited by J. Backman et al., Integrated Ocean Drill. Program Manage. Int., Inc., Edinburgh, doi:10.2204/iodp.proc.302.105.2006.

Moran, K., et al. (2006), The Cenozoic palaeoenvironment of the Arctic Ocean, *Nature*, *441*, 601–605.

Mosbrugger, V., T. Utescher, and D. L. Dilcher (2005), Cenozoic continental climatic evolution of central Europe, *Proc. Natl. Acad. Sci. U.S.A.*, *102*, 14,964–14,969.

Mudie, P. J. (1980), Palynology of later Quaternary marine sediments, eastern Canada, Ph.D. thesis, 638 pp., Dalhousie Univ., Halifax, Nova Scotia, Canada.

Mudie, P. J. (1982), Pollen distribution in recent marine sediments, eastern Canada, *Canadian J. Earth Sci.*, *19*, 729–747.

Pokrovsky, O. S., and J. Schott (2002), Iron colloids/organic matter associated transport of major and trace elements in small boreal rivers and their estuaries (NW Russia), *Chem. Geol.*, *190*, 141–179.

Rohrman, M., and P. A. van der Beek (1996), Cenozoic post-rift domal uplift of North Atlantic margins: An asthenospheric diapirism model, *Geology*, *24*, 901–904.

Sangiorgi, F., H. Brinkhuis, and S. P. Damassa (2008), *Arcticacysta*: A new organic-walled dinoflagellate cyst genus from the early Miocene? of the central Arctic Ocean, *Micropaleontology*, in press.

Schnetger, B. (1997), Trace element analysis of sediments by HR-ICP-MS using low and medium resolution and different acid digestions, *Fresenius J. Anal. Chem.*, *359*, 468–472.

Schouten, S., E. C. Hopmans, E. Schefuß, and J. S. Sinninghe Damsté (2002), Distributional variations in marine crenarchaeotal membrane lipids: A new organic proxy for reconstructing ancient sea water temperatures?, *Earth Planet. Sci. Lett.*, *204*, 265–274.

Schouten, S., C. Huguet, E. C. Hopmans, and J. S. Sinninghe Damsté (2007), Improved analytical methodology of the TEX86 paleothermometry by high performance liquid chromatography/atmospheric pressure chemical ionization-mass spectrometry, *Anal. Chem.*, *79*, 2940–2944.

Schrader, H.-J., and J. Fenner (1976), Norwegian Sea Cenozoic diatom biostratigraphy and taxonomy, *Initial Rep. Deep Sea Drill. Proj.*, *38*, 921–1099.

Sluijs, A., H. Brinkhuis, C. E. Stickley, J. Warnaar, G. L. Williams, and M. Fuller (2003), Dinoflagellate cysts from the Eocene/Oligocene transition in the Southern Ocean: Results from ODP Leg 189, in, *Proc. Ocean Drill. Program, Sci. Results*, 1–42.

Sluijs, A., J. Pross, and H. Brinkhuis (2005), From greenhouse to icehouse: Organic-walled dinoflagellate cysts as paleoenvironmental indicators in the Paleogene, *Earth Sci. Rev.*, *68*, 281–315.

Sluijs, A., et al. (2006), Subtropical Arctic Ocean temperatures during the Palaeocene/Eocene thermal maximum, *Nature*, *441*, 610–613.

Sluijs, A., U. Röhl, S. Schouten, H.-J. Brumsack, F. Sangiorgi, J. S. Sinninghe Damsté, and H. Brinkhuis (2008), Arctic late Paleocene–early Eocene paleoenvironments with special emphasis on the Paleocene-Eocene thermal maximum (Lomonosov Ridge, Integrated Ocean Drilling Program Expedition 302), *23*, PA1S11, doi:10.1029/2007PA001495.

Stein, R., B. Boucsein, and H. Meyer (2006), Anoxia and high primary production in the Paleogene central Arctic Ocean: First detailed records from Lomonosov Ridge, *Geophys. Res. Lett.*, *33*, L18606, doi:10.1029/2006GL026776.

Stickley, C., N. Koç, H.-J. Brumsack, R. Jordan, and I. Suto (2008), A siliceous microfossil view of middle Eocene Arctic paleoenvironments: A window of biosilica production and preservation, *Paleoceanography*, doi:10.1029/2007PA001485, in press.

Tsikalas, F., J. I. Faleide, O. Eldholm, and J. Wilson (2005), Late Mesozoic-Cenozoic structural and stratigraphic correlations between the conjugate mid-Norway and NE Greenland continental margins, in *Petroleum Geology: North-West Europe and Global Perspectives*: *Proceedings of the 6th Petroleum Geology Conference*, vol. 2, edited by A. G. Doré and B. Vining, pp. 785–801, Geol. Soc., London.

Wedepohl, K. H. (1971), Environmental influence on the chemical composition of shales and clays, in *Physics and Chemistry of the Earth*, vol. 8, edited by L. H. Ahrens et al., pp. 305–333, Pergamon, Oxford.

Williams, G. L., and S. B. Manum (1999), Oligocene-early Miocene dinocyst stratigraphy of Hole 985A (Norwegian Sea), *Proc. Ocean Drill. Program Sci. Results*, *162*, 99–109.

Wood, G. D., A. M. Gabriel, and J. C. Lawson (1996), Palynological techniques: Processing and microscopy, in *Palynology: Principles and Applications*, vol. 1, edited by J. Jansonius and D. C. McGregor, chap. 3, pp. 29–50, Am. Assoc. of Stratigr. Palynol. Found., Dallas, Tex.

Zachos, J., M. Pagani, L. Sloan, E. Thomas, and K. Billups (2001), Trends, rhythms, and aberrations in global climate 65 Ma to present, *Science*, *292*, 686–693.

H. Brinkhuis and F. Sangiorgi, Laboratory of Palaeobotany and Palynology, Utrecht University, Budapestlaan 4, 3584 CD Utrecht, Netherlands.

H.-J. Brumsack, Institute for Chemistry and Biology of the Marine Environment (ICBM), Oldenburg University, P.O. Box 2503, D-26111 Oldenburg, Germany.

M. O'Regan, Graduate School of Oceanography University of Rhode Island, Narragansett, RI 02882, USA.

G.-J. Reichart, Department of Earth Sciences, Utrecht University, Budapestlaan 4, 3584 CD Utrecht, Netherlands.

S. Schouten and J. S. Sinninghe Damsté, Royal Netherlands Institute for Sea Research (NIOZ), Department of Marine Biogeochemistry and Toxicology, P.O. Box 59, 1790 AB, Den Burg, Texel, Netherlands.

C. E. Stickley, Norwegian Polar Institute, Polar Environmental Centre, N-9296 Tromsø, Norway.

D. A. Willard, U.S. Geological Survey, 926A National Centre, Reston, VA 20192, USA.